Robotica: (2020) volume 38, pp. 1064–1081. © Cambridge University Press 2019
doi:10.1017/S0263574719001255

# Optimal Design of the Three-Degree-of-Freedom Parallel Manipulator in a Spray-Painting Equipment

Guang Yu†‡, Jun Wu†‡*, Liping Wang†‡ and Ying Gao†‡

†*Department of Mechanical Engineering, State Key Laboratory of Tribology and Institute of Manufacturing Engineering, Tsinghua University, Beijing 100084, China.*
*E-mails: gyu@tsinghua.edu.cn, Lpwang@tsinghua.edu.cn, gaoyingxue2011@163.com*
‡*Beijing Key Lab of Precision/Ultra-precision Manufacturing Equipment and Control, Beijing, China*

(Accepted July 18, 2019. First published online: August 15, 2019)

**SUMMARY**
Spray-painting equipments are important for the automatic spraying of long conical objects such as rocket fairing. This paper proposes a spray-painting equipment that consists of a feed worktable, a gantry frame and two serial–parallel mechanisms and investigates the optimal design of PRR–PRR parallel manipulator in serial–parallel mechanisms. Based on the kinematic model of the parallel manipulator, the conditioning performance, workspace and accuracy performance indices are defined. The dynamic model is derived using virtual work principle and dynamic evaluation index is defined. The conditioning performance, workspace, accuracy performance and dynamic performance are involved in multi-objective optimization design to determine the optimal geometrical parameters of the parallel manipulator. Furthermore, the geometrical parameters of the gantry frame are optimized. An example is given to show how to determine these parameters by taking a long object with conical surface as painted object.

KEYWORDS: Dynamic performance; Genetic algorithm; Multi-objective optimization; Parallel manipulator; Workspace.

## Nomenclature

| | | | |
|---|---|---|---|
| $A_1, A_2$ | slider | $B_1B_2$ | moving platform |
| $A_iB_i$ | link $i$ = 1,2 | $C$-$uv$ | body coordinate system |
| $C$ | center of gravity of $B_1B_2$ | $u,v$ | axis |
| $B_i$ | point $i$ = 1,2 | $A_i$ | point $i$ = 1,2 |
| $O$-$XY$ | fixed coordinate system | $l$ | length of the moving platform |
| $l_i$ | length of link $A_iB_i$ | $\boldsymbol{w}_i$ | unit vector of link $AiB_i$ |
| $w_i$ | angular velocity of link $A_iB_i$ | $x_{ai}$ | $X$ coordinate of point $A_i$ |
| $\boldsymbol{b}_i'$ | vector from point $B_i$ to $C$ in $C$-$uv$ | $\boldsymbol{b}_i$ | vector from point $B_i$ to $C$ in $O$-$XY$ |
| $\boldsymbol{r}$ | position vector of point $C$ | $\boldsymbol{R}$ | rotation matrix from $C$-$uv$ to $O$-$XY$ |
| $\theta_i$ | rotational angle of link $A_iB_i$ | $\boldsymbol{r}_i$ | vector of the mass center of link $A_iB_i$ |
| $\dot{\boldsymbol{r}}$ | velocity vector of point $C$ | $\tilde{\boldsymbol{J}}$ | Jacobian matrix |

* Corresponding author. E-mail: jhwu@mail.tsinghua.edu.cn

| | | | |
|---|---|---|---|
| $\dot{\alpha}$ | rotational angle velocity of moving platform | $\alpha$ | rotational angle of the moving platform |
| $\varepsilon_i$ | angular acceleration of link $A_iB_i$ | $\dot{x}_{ai}$ | $X$ coordinate velocity of point $A_i$ |
| $\ddot{\alpha}$ | rotational angle accelerated velocity of moving platform | $\ddot{x}_{ai}$ | $X$ coordinate accelerated velocity of point $A_i$ |
| $\ddot{r}$ | accelerated velocity vector of point $C$ | $F_{ai}$ | inertia force imposed on slider $A_i$ |
| $m_{ai}$ | mass of slider $A_i$ | $g$ | gravitational acceleration |
| $I_i$ | moment of inertia of link $A_iB_i$ | $m$ | mass of moving platform |
| $\beta$ | angle between the frame and the horizontal plane | $I$ | moment of inertia of moving platform |
| $F_{A1}$ | driving forces imposed on slides $A_1$ | $F_{A2}$ | driving forces imposed on slides $A_2$ |
| $M_\theta$ | driving moment imposed on link $A_1B_1$ | $L$ | length of the guide way |
| $y_{\max}$ | $y$ coordinates of mass center of moving platform when it reaches its upper limits | $y_{\min}$ | $y$ coordinates of mass center of moving platform when it reaches its lower limits |
| $\kappa_J$ | condition number | $\eta_J$ | global performance index |
| $\sigma_1$ | minimum singular values of the Jacobian matrix associated with a given posture | $\sigma_2$ | maximum singular values of the Jacobian matrix associated with a given posture |
| $W$ | workspace | $\Delta y$ | workspace performance |
| $\lambda_i$ | $u$ coordinate of unit vector from point $B_i$ to $C$ in $C$-$uv$ | $\tilde{\boldsymbol{J}}_E$ | error transformation matrix |
| $\delta x_{a1}$ | error of point $A_1$ | $\delta x_{a2}$ | error of point $A_2$ |
| $\delta l_1$ | error of $l_1$ | $\delta l$ | error of $l$ |
| $\delta l_2$ | error of $l_2$ | $\delta \boldsymbol{r}$ | error of $\boldsymbol{r}$ |
| $\delta\alpha$ | error of $\alpha$ | $\delta\theta_2$ | error of $\theta_2$ |
| $\delta\theta_1$ | error of $\theta_1$ | $\kappa_E$ | Ccondition number of $\tilde{\boldsymbol{J}}_E$ |
| $\eta_E$ | accuracy index | $\sigma_{HM}$ | harmonic mean of $\sigma_{\max}$ and $\sigma_{\min}$ |
| $\sigma_{\max}$ | maximum singular values of $\tilde{M}^{-1}$ | $\sigma_{\min}$ | minimum singular values of $\tilde{\boldsymbol{M}}^{-1}$ |
| $\alpha_{\min}$ | minimum rotational angle of the moving platform | $\alpha_{\max}$ | maximum of rotational angle of the moving platform |
| $\Gamma_{HM}$ | dynamic performance | $f_i$ | objective optimization function |
| $\mu_i$ | weight placed upon $f_i$ | $W_d$ | design space |
| $\eta_{E\max}$ | maximum values of $\eta_E$ | $\eta_{E\min}$ | minimum values of $\eta_E$ |
| $\Gamma_{HM\max}$ | maximum values of $\Gamma_{HM}$ | $\Gamma_{HM\min}$ | minimum values of $\Gamma_{HM}$ |
| $\eta_{J\max}$ | maximum values of $\eta_J$ | $\eta_{J\min}$ | minimum values of $\eta_J$ |

## 1. Introduction

With the rapid progress of astronautical technology, the development of large-scale and high-thrust launch vehicle is the inevitable trend. The fairing is an important part of the rocket and its heat-insulating design is indispensable. The traditional layer-skinning method is not suitable for large and complex surfaces, due to its inefficiency and inconvenience to change layer's thickness and shape. Another popular method, spray-painting method, is favored by factories. Traditional manual spraying cannot guarantee the quality and efficiency and is harmful to the operator's health. Spraying manipulator is a good replacement for manual spraying. Taking ABB company as an example, most spraying manipulators are based on series mechanism, and driving motors are installed at each joint from the base to the wrist, which results in large and heavy "arms". The manipulators have poor load capacity and are especially not suitable for spraying large curved surface. Parallel manipulators have attracted interest of researchers because they have high load-to-weight ratio, compact structure and low inertia over the conventional serial manipulators that are constituted with rigid body links and joints connected in serial. Therefore, they are widely used in many applications, such as machine tools, flying machines and assembling robots.[1,2] As an important branch of parallel manipulators, planar parallel manipulators that manipulate an object on a plane also possess the advantages of

https://doi.org/10.1017/S0263574719001255 Published online by Cambridge University Press

general parallel manipulators. Moreover, they have such extra advantages as the simplicity in structure and cost reduction in manufacture. Thus, planar parallel manipulators have been intensively studied, including structural optimization,[3] static and dynamic performance[4–6] and high-accuracy control.[7]

Most studies on planar parallel robots concentrate on the fully parallel ones, with three legs connecting the moving platform to the base.[8] A 3-RRR parallel manipulator, which has three degrees of freedom (DOFs) and eight links, is the most common architecture for a planar 3-DOF parallel manipulator.[9] However, the motion offered by the planar parallel manipulator is rather small because of limitations in the joints and the actuators. This becomes a challenging issue when the desired range of motion for orientation of the moving platform is large. To overcome these problems, Ji[10] proposed a 3-DOF RRR–RRR parallel manipulator. This design sacrifices some rigidity by reducing the parallelism in return for increased functional workspace. Based on the consideration for increased functional workspace, Ider[11] constructed a 2-RPR parallel manipulator by removing the third leg of a 3-RPR parallel manipulator and adding an active actuator to one leg.

Optimal design is an important issue in the development of parallel manipulators. Kinematic design is primarily concerned with the determination of the dimensions of the geometrical parameters and the range of the actuated joint variables.[12–14] The approaches of kinematic design of parallel manipulators may be classified into two categories. One category is the objective function method that involves establishing an objective function and obtaining a result by means of an optimization algorithm.[15,16] Genetic algorithm is one of the most popular algorithms for its parallel computation and global search capacity. However, one of the main drawbacks of genetic algorithm is that the numerical procedure may converge toward to a local optimum.[17] The other category is the performance atlas method[18] that graphically and globally shows the relationship between performance indices and designed parameters. The performance atlas method is suitable for dimensionless optimization, which is only limited to kinematics optimization. Whatever the design method is used, the performance evaluation is involved. The most common evaluation index is the condition number of the Jacobian matrix and the global conditioning index.[19–21] One drawback is that the condition number does not have a physical sense when these indices are applied to optimal design of mixed-DOF parallel manipulators.[22] Based on the concept of transmission angle in a planar mechanism, Wu et al.[23] and Liu et al.[24] proposed the local transmission index and the global transmission index to evaluate the performance of parallel manipulators. However, these designs do not take the dynamic performance into account which is generally considered after the kinematic design. In addition, the accuracy performance is usually not considered in optimal design, which is usually guaranteed by tolerance as well as kinematic calibration after the dimensions are determined. It is important to take the kinematic, accuracy and dynamic performance into account in the first phase of optimal design.

In this paper, a spray-painting equipment for painting objects with conical surface is proposed and the optimal design of the PRR–PRR parallel manipulator in the spray-painting equipment is investigated. This paper is organized as follows. Section 2 addresses the architecture of the spray-painting equipment. Section 3 derives the dynamic model of the PRR–PRR parallel manipulator. Section 4 gives the performance evaluation indices, which are involved in the optimal design in Section 5. The conclusions are drawn in Section 6.

## 2. Architecture and Kinematic Analysis

### *2.1. System architecture*

Some long conical objects (e.g., rocket fairing) have complex surfaces and it is a difficult task to realize the automatic spray-painting of their surfaces. In order to paint a long object with conical surface, at least two rotational DOFs and three translational DOFs are required for a spray-painting equipment. In this paper, a 5-DOF spray-painting equipment shown in Fig. 1 is designed to paint long objects with conical surfaces. The equipment is composed of a feed worktable, a gantry frame and two serial–parallel mechanisms. The painted object is attached to the feed worktable. Each serial–parallel mechanism includes a PRR–PRR manipulator and an arm with one rotational DOF that carries the spray gun. Here, P and R denote the prismatic and rotational joints and the underlined P and R represent the active prismatic and rotational joints, respectively. The rotational arm is attached to the moving platform of the PRR–PRR parallel manipulator. Although the PRR–PRR parallel

https://doi.org/10.1017/S0263574719001255 Published online by Cambridge University Press

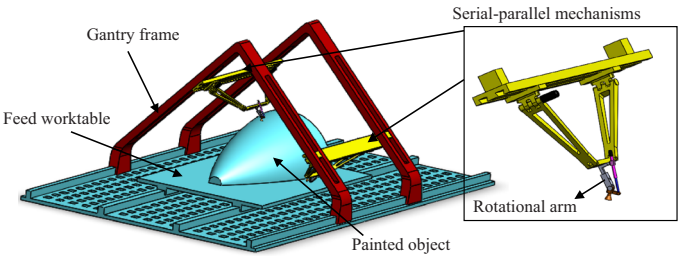


Fig. 1. 3D model of the spray-painting equipment.

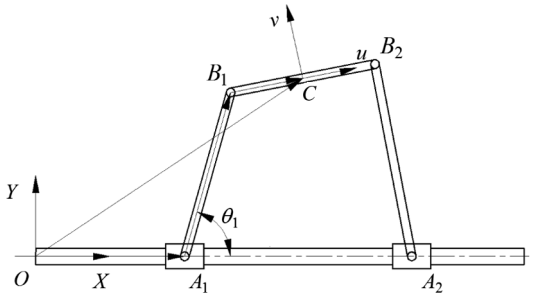


Fig. 2. Schematic diagram of the parallel manipulator.

manipulator is asymmetric, the functional workspace is increased, compared with the fully parallel manipulator with three legs connecting the moving platform to the base. The dimensions of the gantry frame and feed worktable can be determined based on the dimension of the conical surface. Thus, this paper focuses on the optimal design of the PRR–PRR parallel manipulator.

### *2.2. Kinematics*

A schematic diagram of the 3-DOF parallel manipulator is shown in Fig. 2. It is composed of a platform linked to the base by two PRR chains. Sliders $A_1$ and $A_2$ are driven by servomotor-lead screw assembly. One end of link $A_1B_1$ is actuated by one servomotor. A fixed coordinate system $O$–$XY$ with the $X$ and $Y$ axes being horizontally and vertically placed is established on the base. The parallel manipulator is of large dimension and the arm that carries the spraying gun can be ignored. For dynamic characteristics, the position of the spraying gun will affect the inertia distribution. Since the mass of the spraying gun is relatively small compared with the whole serial and parallel mechanism, it can be ignored. It can be considered that the center of gravity is approximately at point $C$ (the center of gravity of $B_1B_2$). So the end of the spraying gun can be thought to be located at the center $C$ of the moving platform $B_1B_2$ approximately. A body coordinate system $C$-$uv$ is attached to the moving platform and the $u$ axis is along the axial axis of moving platform.

The closed-loop constraint equation associated with each chain can be written as:

$$\boldsymbol{r} = x_{ai}\boldsymbol{e}_1 + l_i\boldsymbol{w}_i + \boldsymbol{b}_i, \quad i = 1, 2 \tag{1}$$

where $l_i$ and $\boldsymbol{w}_i$ are the length and unit vector of link $A_iB_i$, $\boldsymbol{r}$ is the position vector of point $C$, $\boldsymbol{b}_i$ is the vector from point $B_i$ to $C$ in $O$-$XY$, $\boldsymbol{b}_i = \boldsymbol{R}\boldsymbol{b}_i'$ and $\boldsymbol{b}_i'$ denotes the vector from point $B_i$ to $C$ in $C$-$uv$, $\boldsymbol{R}$ is the rotation matrix from $C$-$uv$ to $O-XY$, $\boldsymbol{R} = \begin{bmatrix} \cos\alpha & -\sin\alpha \\ \sin\alpha & \cos\alpha \end{bmatrix}$, $\alpha$ is the rotational angle of the moving platform, $x_{ai}$ is the $X$ coordinate of point $A_i$ in $O$-$XY$ and $\boldsymbol{e}_1 = [1\ 0]^T$.

By taking the dot product with $\boldsymbol{e}_1^{\mathrm{T}}$ on both sides of Eq. (1), the position of slider can be expressed as

$$x_{ai} = \boldsymbol{e}_1^{\mathrm{T}}\boldsymbol{r} - \boldsymbol{e}_1^{\mathrm{T}}\boldsymbol{b}_i - l_i\boldsymbol{e}_1^{\mathrm{T}}\boldsymbol{w}_i, \quad i = 1, 2 \tag{2}$$

Then, $\boldsymbol{w}_i$ can be obtained by

$$\boldsymbol{w}_i = \frac{\boldsymbol{r} - x_{ai}\boldsymbol{e}_1 - \boldsymbol{b}_i}{l_i} \tag{3}$$

https://doi.org/10.1017/S0263574719001255 Published online by Cambridge University Press

Let $\theta_i$ and $l$ be the rotational angle of link $A_iB_i$ and length of moving platform, respectively. Taking $\boldsymbol{w}_1 = [\cos\theta_1 \ \ \sin\theta_1]^{\mathrm{T}}$ and the assembly mode into account, $\theta_1$ can be expressed as

$$\theta_1 = \sin^{-1}\frac{2\boldsymbol{e}_2^{\mathrm{T}}\boldsymbol{r} - l\sin\alpha}{2l_1} \quad \text{or} \quad \theta_1 = \pi - \sin^{-1}\frac{2\boldsymbol{e}_2^{\mathrm{T}}\boldsymbol{r} - l\sin\alpha}{2l_1} \tag{4}$$

where $\boldsymbol{e}_2 = [0\ 1]^{\mathrm{T}}$.

The position vector of the mass center of link $A_iB_i$ in coordinate system $O$-$XY$ can be expressed as

$$\boldsymbol{r}_i = \begin{bmatrix} x_i \\ y_i \end{bmatrix} = x_{ai}\boldsymbol{e}_1 + \frac{l_i}{2}\boldsymbol{w}_i, \quad i = 1, 2 \tag{5}$$

*2.3. Jacobian matrix and singularity*

The variables $\boldsymbol{r}$, $x_{ai}$, $\boldsymbol{w}_i$ and $\boldsymbol{b}_i$ exist in the time domain. Taking the derivative of Eq. (1) with respect to time yields

$$\dot{\boldsymbol{r}} = \dot{x}_{ai}\boldsymbol{e}_1 + l_i\omega_i\boldsymbol{E}\boldsymbol{w}_i + \dot{\alpha}\boldsymbol{E}\boldsymbol{b}_i, \quad i = 1, 2 \tag{6}$$

where $\boldsymbol{E} = \begin{bmatrix} 0 & -1 \\ 1 & 0 \end{bmatrix}$ and $w_i$ is the angular velocity of link $A_iB_i$.

Taking the dot product with $\boldsymbol{w}_i^{\mathrm{T}}$ on both sides of Eq. (6) yields

$$\dot{x}_{ai} = \begin{bmatrix} \dfrac{\boldsymbol{w}_i^{\mathrm{T}}}{\boldsymbol{w}_i^{\mathrm{T}}\boldsymbol{e}_1} & \dfrac{-\boldsymbol{w}_i^{\mathrm{T}}\boldsymbol{E}\boldsymbol{b}_i}{\boldsymbol{w}_i^{\mathrm{T}}\boldsymbol{e}_1} \end{bmatrix} \begin{bmatrix} \dot{\boldsymbol{r}} \\ \dot{\alpha} \end{bmatrix} = \boldsymbol{J}_i\dot{\boldsymbol{p}} \tag{7}$$

where $\boldsymbol{J}_i = \begin{bmatrix} \frac{\boldsymbol{w}_i^{\mathrm{T}}}{\boldsymbol{w}_i^{\mathrm{T}}\boldsymbol{e}_1} & \frac{-\boldsymbol{w}_i^{\mathrm{T}}\boldsymbol{E}\boldsymbol{b}_i}{\boldsymbol{w}_i^{\mathrm{T}}\boldsymbol{e}_1} \end{bmatrix}$ and $\dot{\boldsymbol{p}} = \begin{bmatrix} \dot{\boldsymbol{r}} \\ \dot{\alpha} \end{bmatrix}$.

Taking the dot product with $\boldsymbol{e}_2^{\mathrm{T}}$ on both sides of Eq. (6) leads to

$$\omega_i = \begin{bmatrix} \dfrac{\boldsymbol{e}_2^{\mathrm{T}}}{l_i\boldsymbol{e}_2^{\mathrm{T}}\boldsymbol{E}\boldsymbol{w}_i} & \dfrac{-\boldsymbol{e}_2^{\mathrm{T}}\boldsymbol{E}\boldsymbol{b}_i}{l_i\boldsymbol{e}_2^{\mathrm{T}}\boldsymbol{E}\boldsymbol{w}_i} \end{bmatrix} \begin{bmatrix} \dot{\boldsymbol{r}} \\ \dot{\alpha} \end{bmatrix} = \boldsymbol{J}_{\omega i}\dot{\boldsymbol{p}} \tag{8}$$

where $\boldsymbol{J}_{\omega i} = \begin{bmatrix} \frac{\boldsymbol{e}_2^{\mathrm{T}}}{l_i\boldsymbol{e}_2^{\mathrm{T}}\boldsymbol{E}\boldsymbol{w}_i} & \frac{-\boldsymbol{e}_2^{\mathrm{T}}\boldsymbol{E}\boldsymbol{b}_i}{l_i\boldsymbol{e}_2^{\mathrm{T}}\boldsymbol{E}\boldsymbol{w}_i} \end{bmatrix}$.

Rewriting Eqs. (7) and (8) in matrix format results in the velocity mapping of the 3-DOF parallel manipulator

$$\dot{\boldsymbol{q}} = \boldsymbol{J}\dot{\boldsymbol{p}} \tag{9}$$

where $\boldsymbol{q} = [x_{a1}, x_{a2}, \theta_1]^{\mathrm{T}}$, $\boldsymbol{J}$ is the Jacobian matrix and $\boldsymbol{J} = [\boldsymbol{J}_1, \boldsymbol{J}_2, \boldsymbol{J}_{w1}]^{\mathrm{T}}$.

Jacobi represents the relationship between input velocity and output velocity, and Jacobi's condition number represents the flexibility of mechanism. The closer to 1 the Jacobi's condition number is, the more flexible the mechanism is. In the design of parallel mechanism, if the condition number of the mechanism is large, a very small input velocity will lead to a great output velocity. It brings great difficulties to machining and assembling, and more importantly, it is difficult to control. So the condition number is very important for parallel mechanism. For the parallel manipulator having both translational and rotational DOFs, the units of translational DOFs are not the same as the units of rotational DOFs. To deal with this problem, Ma and Angeles[25] suggested to define a normalized inverse Jacobian matrix by dividing the rotational elements of the matrix by a characteristic length, which is defined by the normalizing length that renders Jacobian matrix dimensionless. In this paper, $l_1$ and $l/2$ are chosen as the characteristic lengths. Let $\tilde{\boldsymbol{q}} = \begin{bmatrix} x_{a1} & x_{a2} & l_1\theta_1 \end{bmatrix}^{\mathrm{T}}$ and $\tilde{\boldsymbol{p}} = \begin{bmatrix} \boldsymbol{r} \\ \alpha\frac{l}{2} \end{bmatrix}$. The Jacobian matrix can be rewritten as

$$\tilde{\boldsymbol{J}} = \begin{bmatrix} 1 & 0 & 0 \\ 0 & 1 & 0 \\ 0 & 0 & l_1 \end{bmatrix} \boldsymbol{J} \begin{bmatrix} 1 & 0 & 0 \\ 0 & 1 & 0 \\ 0 & 0 & \frac{2}{l} \end{bmatrix} \tag{10}$$

https://doi.org/10.1017/S0263574719001255 Published online by Cambridge University Press

Differentiating Eq. (5) with respect to time leads to

$$\dot{\boldsymbol{r}}_i = \left( \begin{bmatrix} \boldsymbol{J}_i \\ 0 \end{bmatrix} + \frac{l_i}{2} \begin{bmatrix} \boldsymbol{e}_1^{\mathrm{T}} \boldsymbol{E} \boldsymbol{w}_i \boldsymbol{J}_{\omega i} \\ \boldsymbol{e}_2^{\mathrm{T}} \boldsymbol{E} \boldsymbol{w}_i \boldsymbol{J}_{\omega i} \end{bmatrix} \right) \begin{bmatrix} \dot{\boldsymbol{r}} \\ \dot{\alpha} \end{bmatrix} = \boldsymbol{J}_{vi} \dot{\boldsymbol{p}} \tag{11}$$

where $\boldsymbol{J}_{vi} = \begin{bmatrix} \boldsymbol{J}_i \\ 0 \end{bmatrix} + \frac{l_i}{2} \begin{bmatrix} \boldsymbol{e}_1^{\mathrm{T}} \boldsymbol{E} \boldsymbol{w}_i \boldsymbol{J}_{\omega i} \\ \boldsymbol{e}_2^{\mathrm{T}} \boldsymbol{E} \boldsymbol{w}_i \boldsymbol{J}_{\omega i} \end{bmatrix}$.

Using the Jacobian matrices-based method, the singular configuration of PRR–PRR parallel manipulator can be determined. When one or more singular values of $\tilde{J}$ are infinite, the inverse kinematic singularity occurs. It can be concluded that this condition is satisfied when one of the links $A_iB_i$ is vertical. This singularity is a boundary singularity. In fact, this configuration is not really singular for this parallel manipulator since link $A_1B_1$ is active. The direct kinematic singularity occurs when one or more singular values of $\tilde{J}$ are zero. For the PRR–PRR parallel manipulator, this type of singularity occurs when links $B_1B_2$ and $A_2B_2$ are collinear.

## 3. Dynamic Analysis

### *3.1. Acceleration analysis*

The variables $\dot{r}$, $\dot{x}_{ai}$, $\boldsymbol{w}_i$, $\dot{\alpha}$ and $\boldsymbol{b}_i$ are described in the time domain. Differentiating Eq. (6) with respect to time yields

$$\ddot{x}_{ai} \boldsymbol{e}_1 + l_i \varepsilon_i \boldsymbol{E} \boldsymbol{w}_i - l_i \omega_i^2 \boldsymbol{w}_i = \ddot{\boldsymbol{r}} - \ddot{\alpha} \boldsymbol{E} \boldsymbol{b}_i + \dot{\alpha}^2 \boldsymbol{b}_i, \quad i = 1, 2 \tag{12}$$

where $\varepsilon_i$ is the angular acceleration of link $A_iB_i$.

Taking the dot product with $\boldsymbol{w}_i^{\mathrm{T}}$ on both sides of Eq. (12) leads to

$$\ddot{x}_{ai} = \begin{bmatrix} \dfrac{\boldsymbol{w}_i^{\mathrm{T}}}{\boldsymbol{w}_i^{\mathrm{T}} \boldsymbol{e}_1} & \dfrac{-\boldsymbol{w}_i^{\mathrm{T}} \boldsymbol{E} \boldsymbol{b}_i}{\boldsymbol{w}_i^{\mathrm{T}} \boldsymbol{e}_1} \end{bmatrix} \begin{bmatrix} \ddot{\boldsymbol{r}} \\ \ddot{\alpha} \end{bmatrix} + \left( \frac{l_i \omega_i}{\boldsymbol{w}_i^T \boldsymbol{e}_1} \boldsymbol{J}_{\omega i} + \begin{bmatrix} 0 & 0 & \dfrac{\boldsymbol{w}_i^{\mathrm{T}} \boldsymbol{b}_i}{\boldsymbol{w}_i^{\mathrm{T}} \boldsymbol{e}_1} \dot{\alpha} \end{bmatrix} \right) \begin{bmatrix} \dot{\boldsymbol{r}} \\ \dot{\alpha} \end{bmatrix} = \boldsymbol{J}_i \ddot{\boldsymbol{p}} + \boldsymbol{H}_i \dot{\boldsymbol{p}} \tag{13}$$

where $\boldsymbol{H}_i = \frac{l_i \omega_i}{\boldsymbol{w}_i^T \boldsymbol{e}_1} \boldsymbol{J}_{\omega i} + \begin{bmatrix} 0 & 0 & \frac{\boldsymbol{w}_i^{\mathrm{T}} \boldsymbol{b}_i}{\boldsymbol{w}_i^{\mathrm{T}} \boldsymbol{e}_1} \dot{\alpha} \end{bmatrix}$.

Taking the dot product with $\boldsymbol{e}_2^{\mathrm{T}}$ on both sides of Eq. (12) leads to

$$\varepsilon_i = \begin{bmatrix} \dfrac{\boldsymbol{e}_2^{\mathrm{T}}}{l_i \boldsymbol{e}_2^{\mathrm{T}} \boldsymbol{E} \boldsymbol{w}_i} & \dfrac{-\boldsymbol{e}_2^{\mathrm{T}} \boldsymbol{E} \boldsymbol{b}_i}{l_i \boldsymbol{e}_2^{\mathrm{T}} \boldsymbol{E} \boldsymbol{w}_i} \end{bmatrix} \begin{bmatrix} \ddot{\boldsymbol{r}} \\ \ddot{\alpha} \end{bmatrix} + \left( \frac{\omega_i \boldsymbol{e}_2^{\mathrm{T}} \boldsymbol{w}_i}{\boldsymbol{e}_2^{\mathrm{T}} \boldsymbol{E} \boldsymbol{w}_i} \boldsymbol{J}_{\omega i} + \begin{bmatrix} 0 & 0 & \dfrac{\boldsymbol{e}_2^{\mathrm{T}} \boldsymbol{b}_i}{l_i \boldsymbol{e}_2^{\mathrm{T}} \boldsymbol{E} \boldsymbol{w}_i} \dot{\alpha} \end{bmatrix} \right) \begin{bmatrix} \dot{\boldsymbol{r}} \\ \dot{\alpha} \end{bmatrix} = \boldsymbol{J}_{\omega i} \ddot{\boldsymbol{p}} + \boldsymbol{H}_{\omega i} \dot{\boldsymbol{p}} \tag{14}$$

where $\boldsymbol{H}_{\omega i} = \frac{\omega_i \boldsymbol{e}_2^{\mathrm{T}} \boldsymbol{w}_i}{\boldsymbol{e}_2^{\mathrm{T}} \boldsymbol{E} \boldsymbol{w}_i} \boldsymbol{J}_{\omega i} + \begin{bmatrix} 0 & 0 & \frac{\boldsymbol{e}_2^{\mathrm{T}} \boldsymbol{b}_i}{l_i \boldsymbol{e}_2^{\mathrm{T}} \boldsymbol{E} \boldsymbol{w}_i} \dot{\alpha} \end{bmatrix}$

By differentiating Eq. (11) with respect to time, the acceleration of the mass center of link $A_iB_i$ can be expressed as

$$\begin{aligned} \ddot{\boldsymbol{r}}_i &= \left( \begin{bmatrix} \boldsymbol{J}_i \\ 0 \end{bmatrix} + \frac{li}{2} \begin{bmatrix} \boldsymbol{e}_1^{\mathrm{T}} \boldsymbol{E} \boldsymbol{w}_i \boldsymbol{J}_{\omega i} \\ \boldsymbol{e}_2^{\mathrm{T}} \boldsymbol{E} \boldsymbol{w}_i \boldsymbol{J}_{\omega i} \end{bmatrix} \right) \begin{bmatrix} \ddot{\boldsymbol{r}} \\ \ddot{\alpha} \end{bmatrix} + \left( \begin{bmatrix} \boldsymbol{H}_i \\ 0 \end{bmatrix} + \frac{l_i}{2} \begin{bmatrix} \boldsymbol{e}_1^{\mathrm{T}} \boldsymbol{E} \boldsymbol{w}_i \boldsymbol{H}_{\omega i} \\ \boldsymbol{e}_2^{\mathrm{T}} \boldsymbol{E} \boldsymbol{w}_i \boldsymbol{H}_{\omega i} \end{bmatrix} - \frac{l_i \omega_i}{2} \begin{bmatrix} \boldsymbol{e}_1^{\mathrm{T}} \boldsymbol{w}_i \boldsymbol{J}_{\omega i} \\ \boldsymbol{e}_2^{\mathrm{T}} \boldsymbol{w}_i \boldsymbol{J}_{\omega i} \end{bmatrix} \right) \begin{bmatrix} \dot{\boldsymbol{r}} \\ \dot{\alpha} \end{bmatrix} \\ &= \boldsymbol{J}_{vi} \ddot{\boldsymbol{p}} + \boldsymbol{H}_{vi} \dot{\boldsymbol{p}} \end{aligned} \tag{15}$$

where $\boldsymbol{H}_{vi} = \begin{bmatrix} \boldsymbol{H}_i \\ 0 \end{bmatrix} + \frac{l_i}{2} \begin{bmatrix} \boldsymbol{e}_1^{\mathrm{T}} \boldsymbol{E} \boldsymbol{w}_i \boldsymbol{H}_{\omega i} \\ \boldsymbol{e}_2^{\mathrm{T}} \boldsymbol{E} \boldsymbol{w}_i \boldsymbol{H}_{\omega i} \end{bmatrix} - \frac{l_i \omega_i}{2} \begin{bmatrix} \boldsymbol{e}_1^{\mathrm{T}} \boldsymbol{w}_i \boldsymbol{J}_{\omega i} \\ \boldsymbol{e}_2^{\mathrm{T}} \boldsymbol{w}_i \boldsymbol{J}_{\omega i} \end{bmatrix}$.

### *3.2. Force analysis*

The inertia force imposed on slider $A_i$ can be expressed as

$$F_{ai} = -m_{ai} \ddot{x}_{ai} \tag{16}$$

where $m_{\mathrm{ai}}$ is the mass of slider $A_i$.

https://doi.org/10.1017/S0263574719001255 Published online by Cambridge University Press

The resultant of inertia and applied forces imposed on the mass center of link $A_iB_i$ can be expressed as

$$\begin{bmatrix} \boldsymbol{F}_i \\ \boldsymbol{N}_i \end{bmatrix} = \begin{bmatrix} m_i\boldsymbol{g} - m_i\ddot{\boldsymbol{r}}_i \\ -I_i\varepsilon_i \end{bmatrix} \tag{17}$$

where $m_i$ is the mass of link $A_iB_i$, $I_i$ is the moment of inertia of link $A_iB_i$ about point $O$ in $O$-$XY$, $\boldsymbol{g} = \begin{bmatrix} 0 \\ g\cos\beta \end{bmatrix}$, $g$ is the gravitational acceleration and $\beta$ is the angle between the frame and the horizontal plane, as shown in Fig. 6.

The resultant of inertia and applied forces imposed on the mass center of moving platform can be written as

$$\begin{bmatrix} \boldsymbol{F} \\ \boldsymbol{N} \end{bmatrix} = \begin{bmatrix} m\boldsymbol{g} - m\ddot{\boldsymbol{r}} \\ -I\ddot{\alpha} \end{bmatrix} \tag{18}$$

where $m$ is the mass of moving platform, $I$ is the moment of inertia of moving platform $B_1B_2$ about point $O$ in $O$-$XY$.

### *3.3. Dynamic model*

Based on the principle of virtual work, the dynamic equation can be expressed as

$$\begin{bmatrix} \delta\boldsymbol{r} \\ \delta\alpha \end{bmatrix}^{\mathrm{T}} \begin{bmatrix} \boldsymbol{F} \\ N \end{bmatrix} + \sum_{i=1}^{2} \left( \begin{bmatrix} \delta\boldsymbol{r}_i \\ \delta\theta_i \end{bmatrix}^{\mathrm{T}} \begin{bmatrix} \boldsymbol{F}_i \\ N_i \end{bmatrix} + \delta x_{ai} F_{ai} \right) + \delta\boldsymbol{q}^{\mathrm{T}}\boldsymbol{\tau} = 0 \tag{19}$$

where $\boldsymbol{\tau}$ is the driving torque provided by the actuators and $\boldsymbol{\tau} = [F_{A1}\ F_{A2}\ M_\theta]^{\mathrm{T}}$, $F_{A1}$ and $F_{A2}$ are the driving forces imposed on slides $A_1$ and $A_2$, and $M_\theta$ is the driving moment imposed on link $A_1B_1$.

Based on Eq. (19), the inverse dynamic equation can be written as

$$\boldsymbol{\tau} = \boldsymbol{M}(\boldsymbol{p})\ddot{\boldsymbol{p}} + \boldsymbol{H}(\boldsymbol{p}, \dot{\boldsymbol{p}})\dot{\boldsymbol{p}} + \boldsymbol{G}(\boldsymbol{p}) \tag{20}$$

where $\boldsymbol{M}(\boldsymbol{p}) = (\boldsymbol{J}^{-1})^{\mathrm{T}} \begin{bmatrix} m & 0 & 0 \\ 0 & m & 0 \\ 0 & 0 & I \end{bmatrix} + \sum_{i=1}^{2} (\boldsymbol{J}^{-1})^{\mathrm{T}} \left( \begin{bmatrix} \boldsymbol{J}_{vi}^{\mathrm{T}} & \boldsymbol{J}_{\omega i}^{\mathrm{T}} \end{bmatrix} \begin{bmatrix} m_i & 0 & 0 \\ 0 & m_i & 0 \\ 0 & 0 & I_i \end{bmatrix} \begin{bmatrix} \boldsymbol{J}_{vi} \\ \boldsymbol{J}_{\omega i} \end{bmatrix} + m_{ai}\boldsymbol{J}_i^{\mathrm{T}}\boldsymbol{J}_i \right)$,

$$\boldsymbol{H}(\boldsymbol{p}, \dot{\boldsymbol{p}}) = \sum_{i=1}^{2} (\boldsymbol{J}^{-1})^{T} \left( \begin{bmatrix} \boldsymbol{J}_{vi}^{\mathrm{T}} & \boldsymbol{J}_{\omega i}^{\mathrm{T}} \end{bmatrix} \begin{bmatrix} m_i & 0 & 0 \\ 0 & m_i & 0 \\ 0 & 0 & I_i \end{bmatrix} \begin{bmatrix} \boldsymbol{H}_{vi} \\ \boldsymbol{H}_{\omega i} \end{bmatrix} + m_{ai}\boldsymbol{J}_i^{\mathrm{T}}\boldsymbol{H}_i \right),$$

$$\boldsymbol{G}(\boldsymbol{p}) = (\boldsymbol{J}^{-1})^{\mathrm{T}} \begin{bmatrix} -m\boldsymbol{g} \\ 0 \end{bmatrix} + \sum_{i=1}^{2} (\boldsymbol{J}^{-1})^{\mathrm{T}} \left( \begin{bmatrix} \boldsymbol{J}_{vi}^{\mathrm{T}} \boldsymbol{J}_{\omega i}^{\mathrm{T}} \end{bmatrix} \begin{bmatrix} -m\boldsymbol{g} \\ 0 \end{bmatrix} \right).$$

## 4. Performance Indices

Workspace and conditioning performance are general performances for a painting robot and they are considered in the optimal design. Accuracy is a crucially important performance specification of parallel manipulator, particularly for those used as automatic painting robots. In addition, the dynamic performance is one of the most important factors to be taken into account. Therefore, accuracy and dynamic performance are also taken into account in the optimal design.

### *4.1. Workspace*

For the 3-DOF parallel manipulator, there are three variables $x$, $y$ and $\alpha$ to determine the position and pose workspace. The position workspace of the mechanism is a region of the plane that can be obtained by determining the workspace of the reference point $C$ in the center of the moving platform. Let $L$ be the length of the guide way. The letters signed with subscript "up" or "low" mean the configuration that reaches upper bound or lower bound, respectively. The letters signed with superscript "′" or without "′" mean the configuration that reaches right or left bound, respectively.

For a certain angle $\alpha(\alpha > 0°)$, the workspace of $X$–$Y$ plane is shown in Fig. 3. Based on the investigation of singular configuration, the reference point $C$ reaches its upper limits when one link

https://doi.org/10.1017/S0263574719001255 Published online by Cambridge University Press

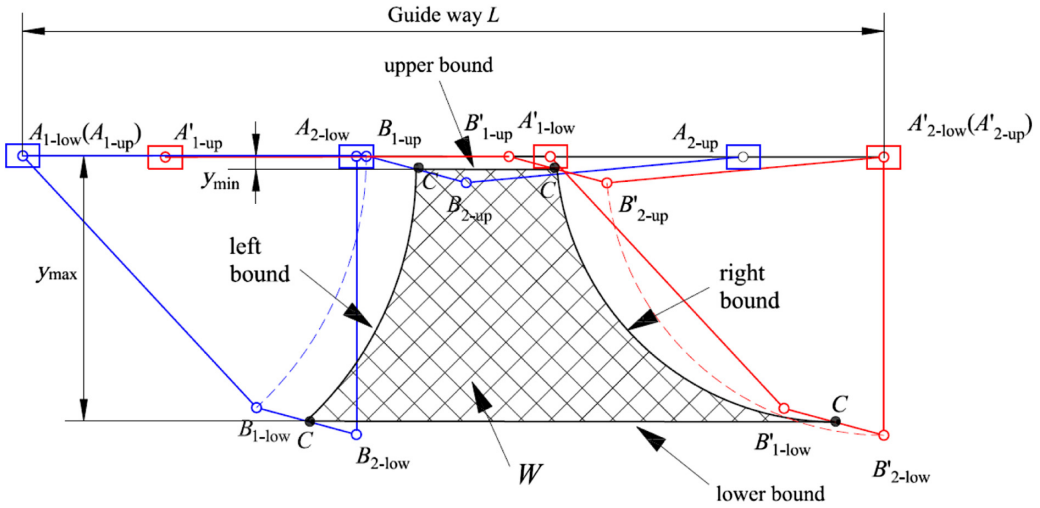


Fig. 3. Workspace of the 3-DOF parallel manipulator.

$A_iB_i$ is parallel to the guide way. The reference point $C$ reaches its lower limits when one link $A_iB_i$ is perpendicular to the guide way. Given $l_1$, $l$, $l_2$ and $L$, the upper and lower bound can be obtained easily. The left and right workspace bound of point $C$ in $X$–$Y$ plane can be determined by the left and right workspace bound of points $B_1$ and $B_2$ since the rotational angle $\alpha$ is specified in Fig. 3. Left workspace bound of point $B_1$ is an arc $B_{1-low}B_{1-up}$ with $A_{1-low}(A_{1-up})$ being the center and $l_1$ being the radius as $A_1$ reaches the left edge of the guide way. Accordingly, the left workspace bound of point $C$ can be determined, as shown in Fig. 3. In this same way, the right workspace bound of point $C$ can be found as $A_2$ reaches the right edge of the guide way. The boundary can be expressed as follows:

$$\text{Upper boundary:} \quad y = \frac{l}{2}\sin\alpha \tag{21}$$

$$\text{Lower boundary:} \quad y = l_2 - \frac{l}{2}\sin\alpha \tag{22}$$

$$\text{Left boundary:} \quad y = \sqrt{l_1^2 - \left(x - \frac{l}{2}\cos\alpha\right)^2} + \frac{l}{2}\sin\alpha \tag{23}$$

$$\text{Right boundary:} \quad y = \sqrt{l_2^2 - \left(x - L + \frac{l}{2}\cos\alpha\right)^2} - \frac{l}{2}\sin\alpha \tag{24}$$

It is easy to find that the motion range of $X$ direction is mostly determined by the length of the guide way and can be improved by the coordinated motion of the sprayed object. So only the range of $y$, $\alpha$ is to find to determine the workspace. Let $y_{\max}$ and $y_{\min}$ be the $y$ coordinates of mass center of moving platform when it reaches its upper and lower limits. Y depends on $\alpha$ and $y_{\max}$ and $y_{\min}$ can be determined when $\alpha$ is given. Accordingly, the following parametric relationships can be generated.

When $\alpha > 0°$ and $l_2 \geq l_1 + l\sin\alpha$, $y_{\max}$ and $y_{\min}$ are determined by

$$y_{\max} = l_1 + \frac{l}{2}\sin\alpha, \quad y_{\min} = \frac{l}{2}\sin\alpha \tag{25}$$

When $\alpha > 0°$ and $l\sin\alpha < l_2 < l_1 + l\sin\alpha$, the range of $y$ is given by

$$y_{\max} = l_2 - \frac{l}{2}\sin\alpha, \quad y_{\min} = \frac{l}{2}\sin\alpha \tag{26}$$

When $\alpha < 0°$ and $l_1 \geq l_2 - l\sin\alpha$, $y_{\max}$ and $y_{\min}$ are determined by

$$y_{\max} = l_2 - \frac{l}{2}\sin\alpha, \quad y_{\min} = \left(-l_2 - \frac{l}{2}\right)\sin\alpha \tag{27}$$

https://doi.org/10.1017/S0263574719001255 Published online by Cambridge University Press

When $\alpha < 0^\circ$ and $-(l+l_2)\sin\alpha < l_1 < l_2 - l\sin\alpha$, the range of $y$ is given by

$$y_{\max} = l_1 + \frac{l}{2}\sin\alpha, \quad y_{\min} = \left(-l_2 - \frac{l}{2}\right)\sin\alpha \tag{28}$$

For a given $\alpha$, $\Delta y = y_{\max} - y_{\min}$ can be used to evaluate the workspace. When $\alpha$ ranges from its lower limit $\alpha_{\min}$ to upper limit $\alpha_{\max}$, the average value of $\Delta y$ can evaluate the workspace performance. Namely,

$$\Delta\bar{y} = \frac{\int \Delta y d\alpha}{\int d\alpha} \tag{29}$$

The bigger the value of $\Delta y$, the larger the workspace of the manipulator.

### *4.2. Conditioning performance*

The condition number of Jacobian matrix is the most frequently used index to evaluate the velocity, accuracy and rigidity mapping characteristics between the joint variables and the moving platform. The condition number $\kappa_J$ is defined as

$$1 \le \kappa_J = \frac{\sigma_2}{\sigma_1} \le \infty \tag{30}$$

where $\sigma_1$ and $\sigma_2$ are the minimum and maximum singular values of the Jacobian matrix associated with a given posture.

The condition number $\kappa_J$ ranges from 1 to 8. In a pose where $\kappa_J$ is equal to 1, the dexterity of the manipulator is best and the manipulator is isotropic. Designing a parallel manipulator that is isotropic in one pose or over its full workspace is often considered as a design objective. Since the condition number $\kappa_J$ is configuration-dependent, a global performance index $\eta_J$ is used as the performance measure, namely

$$\eta_J = \int_W \frac{1}{\kappa_J} dW \Big/ \int_W dW \tag{31}$$

where $W$ is the workspace.

Based on Eq. (31), one may see that $\eta_J$ varies from 0 to 1. The bigger the value of $\eta_J$, the better the dexterity of the manipulator.

### *4.3. Accuracy performance*

By differentiating Eq. (1), the differential error model can be written as

$$\delta x_{ai}\boldsymbol{e}_1 + \delta l_i \boldsymbol{w}_i + l_i \delta \boldsymbol{w}_i = \delta \boldsymbol{r} - \delta \boldsymbol{R}\boldsymbol{b}_i' - \boldsymbol{R}\delta \boldsymbol{b}_i' \tag{32}$$

where $\delta \boldsymbol{w}_i = \delta\theta_i \boldsymbol{E}\boldsymbol{w}_i$, $\delta \boldsymbol{R} = \delta\alpha \boldsymbol{E}\boldsymbol{R}$ and $\delta \boldsymbol{b}_i' = \frac{\delta l}{2}\begin{bmatrix}\lambda_i \\ 0\end{bmatrix}$. $\lambda_i$ represents the $u$ coordinate of unit vector from point $B_i$ to $C$ in $C$-$uv$, $\lambda_1 = 1$ and $\lambda_2 = -1$.

Here, actuator errors and dimension parameter errors are considered. The error sources include actuation error $\delta\boldsymbol{q} = [\delta x_{a1}\ \delta x_{a2}\ \delta\theta_1]^T$ and link length error $\delta \boldsymbol{l}_e = [\delta l_1\ \delta l\ \delta l_2]^T$, and the vector of platform pose error $\delta \boldsymbol{p} = [\delta \boldsymbol{r}^T\ \delta\alpha]^T$. Let $\delta\theta_2 = 0$ and Eq. (32) can be rewritten as

$$\boldsymbol{K}\delta \boldsymbol{p} = \boldsymbol{J}_q \delta \boldsymbol{q} + \boldsymbol{J}_l \delta \boldsymbol{l}_e = \boldsymbol{H}\delta \boldsymbol{e} \tag{33}$$

where $\delta \boldsymbol{e} = \begin{bmatrix}\delta \boldsymbol{q}^{\mathrm{T}}\ \delta \boldsymbol{l}_e^{\mathrm{T}}\end{bmatrix}^{\mathrm{T}}$, $\boldsymbol{H} = \begin{bmatrix}\boldsymbol{J}_q \vdots \boldsymbol{J}_l\end{bmatrix}$, $\boldsymbol{K} = \begin{bmatrix}\boldsymbol{e}_1^{\mathrm{T}} & -\boldsymbol{e}_1^{\mathrm{T}}\boldsymbol{E}\boldsymbol{R}\boldsymbol{b}_1' \\ \boldsymbol{e}_2^{\mathrm{T}} & -\boldsymbol{e}_2^{\mathrm{T}}\boldsymbol{E}\boldsymbol{R}\boldsymbol{b}_1' \\ \boldsymbol{w}_2^{\mathrm{T}} & -\boldsymbol{w}_2^{\mathrm{T}}\boldsymbol{E}\boldsymbol{R}\boldsymbol{b}_2'\end{bmatrix}$, $\boldsymbol{J}_q = \begin{bmatrix}1 & 0 & l_1\boldsymbol{e}_1^{\mathrm{T}}\boldsymbol{E}\boldsymbol{w}_1 \\ 0 & 0 & l_1\boldsymbol{e}_2^{\mathrm{T}}\boldsymbol{E}\boldsymbol{w}_1 \\ 0 & \boldsymbol{w}_2^{\mathrm{T}}\boldsymbol{e}_1 & 0\end{bmatrix}$, $\boldsymbol{J}_l = \begin{bmatrix}\boldsymbol{e}_1^{\mathrm{T}}\boldsymbol{w}_1 & \frac{\boldsymbol{e}_1^{\mathrm{T}}\boldsymbol{R}\boldsymbol{b}_1'}{l} & 0 \\ \boldsymbol{e}_2^{\mathrm{T}}\boldsymbol{w}_1 & \frac{\boldsymbol{e}_2^{\mathrm{T}}\boldsymbol{R}\boldsymbol{b}_1'}{l} & 0 \\ 0 & \frac{\boldsymbol{w}_2^{\mathrm{T}}\boldsymbol{R}\boldsymbol{b}_2'}{l} & 1\end{bmatrix}$.

https://doi.org/10.1017/S0263574719001255 Published online by Cambridge University Press

If $\det(\boldsymbol{K}) \neq 0$, Eq. (33) can be rewritten as

$$\delta \boldsymbol{p} = \boldsymbol{J}_E \delta \boldsymbol{e} \tag{34}$$

where $\boldsymbol{J}_E = \boldsymbol{K}^{-1}\mathbf{H}$.

Since the error sources and platform pose errors include length errors and angular errors, the elements in $\boldsymbol{J}_E$ have different units. It is necessary to homogenize the units of $\boldsymbol{J}_E$ so as to generate a total error transformation matrix.[26] Let $\delta\tilde{\boldsymbol{e}} = \left[\, \delta \boldsymbol{x}_{a1} \;\; \delta \boldsymbol{x}_{a2} \;\; l_1 \delta\theta_1 \;\; \delta \boldsymbol{l}_e^{\mathrm{T}} \,\right]^{\mathrm{T}}$ and $\delta\tilde{\boldsymbol{p}} = \left[\, \delta \boldsymbol{r}^{\mathrm{T}} \;\; \frac{l}{2}\delta\alpha \,\right]^{\mathrm{T}}$. Eq. (34) can be rewritten as

$$\delta\tilde{\boldsymbol{p}} = \tilde{\boldsymbol{J}}_E \delta\tilde{\boldsymbol{e}} \tag{35}$$

where $\tilde{\boldsymbol{J}}_E = \mathrm{diag}\left(1,\ 1,\ \frac{l}{2}\right)\boldsymbol{J}_E \cdot \mathrm{diag}\left(1,\ 1,\ \frac{1}{l_1},\ 1,\ 1,\ 1\right)$ is the error transformation matrix.

The condition number $\kappa_E$ of the error transformation matrix can be utilized as a measure of the relative error amplification, which also characterizes the isotropy of the error ellipsoid. $\kappa_E$ is defined as

$$\kappa_E = \mathrm{cond}(\tilde{\boldsymbol{J}}_E) \tag{36}$$

The smaller the value of $\kappa_E$, the better the accuracy of the manipulator. Since the condition number $\kappa_E$ of error transformation matrix depends on the mechanism configuration, an accuracy index similar to that proposed by Gosselin and Angeles[3] is used as one of the global performance measures to be minimized in the optimal design of parallel manipulators. It is assumed that $\alpha \in [\alpha_{\min}\alpha_{\max}]$, and the workspace $W$ can be determined. The accuracy index can be expressed as

$$\eta_E = \frac{\int_W \kappa_E dW}{\int_W dW} \tag{37}$$

The smaller the value of $\eta_E$, the better the accuracy of the manipulator.

### *4.4. Dynamic performance*

As addressed in ref. [27], the dynamic performance of a manipulator can be represented by the degree of arbitrariness of changing the acceleration on the actuated joint force. The driving force (torque) needs to change abruptly because of the abrupt change of acceleration, which has an influence on the motion precision of a manipulator. Therefore, the inertia item $\boldsymbol{M}(\boldsymbol{p})\ddot{\boldsymbol{p}}$ in Eq. (20) is the major concern. For the manipulator at a certain pose, the gravity item $\boldsymbol{G}(\boldsymbol{p})$ in Eq. (20) is constant. In addition, the velocity item $\boldsymbol{H}(\boldsymbol{p}, \dot{\boldsymbol{p}})\dot{\boldsymbol{p}}$ (including centrifugal and Coriolis items) can be neglected because there is no Coriolis force for the planar parallel mechanism and the centrifugal item has a little effect on the dynamic model for a low-speed mechanism. Thus, by neglecting velocity item and gravitational item, Eq. (20) can be rewritten in a unified form as

$$\boldsymbol{\tau} \approx \boldsymbol{M}(\boldsymbol{p})\ddot{\boldsymbol{p}} \tag{38}$$

Since the parallel manipulator has both translational and rotational DOFs, the singular value of inertia matrix $\boldsymbol{M}(\boldsymbol{p})$ does not have a physical meaning. The same way to deal with the condition number of Jacobian matrix in Section 2.3 is used. Eq. (38) can be rewritten as

$$\ddot{\tilde{\boldsymbol{p}}} = \tilde{\boldsymbol{M}}^{-1}(\boldsymbol{p})\tilde{\boldsymbol{\tau}} \tag{39}$$

where $\tilde{\boldsymbol{\tau}} = \left[\, F_{A1} \;\; F_{A2} \;\; \frac{M_\theta}{l_1} \,\right]^{\mathrm{T}}$, $\ddot{\tilde{\boldsymbol{p}}} = \left[\, \ddot{x} \;\; \ddot{y} \;\; \frac{l}{2}\ddot{\alpha} \,\right]^{\mathrm{T}}$ and $\tilde{\boldsymbol{M}}(\boldsymbol{p}) = \begin{bmatrix} 1 & 0 & 0 \\ 0 & 1 & 0 \\ 0 & 0 & \frac{1}{l_1} \end{bmatrix} \boldsymbol{M}(\boldsymbol{p}) \begin{bmatrix} 1 & 0 & 0 \\ 0 & 1 & 0 \\ 0 & 0 & \frac{2}{l} \end{bmatrix}$. Let $\sigma_{\max}$ and $\sigma_{\min}$ be the maximum and minimum singular values of $\tilde{\boldsymbol{M}}^{-1}$. The physical meaning of $\sigma_{\max}$ and $\sigma_{\min}$ can be interpreted as the maximum and minimum magnitude of acceleration vector of the moving platform for a unit actuated force. The harmonic mean of $\sigma_{\max}$ and $\sigma_{\min}$ can be written as

$$\sigma_{HM} = \frac{2}{\frac{1}{\sigma_{\max}} + \frac{1}{\sigma_{\min}}} = \frac{2}{1 + cond\left(\tilde{\boldsymbol{M}}^{-1}\right)} \tag{40}$$

where $\sigma_{HM}$ is the harmonic mean of $\sigma_{\max}$ and $\sigma_{\min}$.

https://doi.org/10.1017/S0263574719001255 Published online by Cambridge University Press

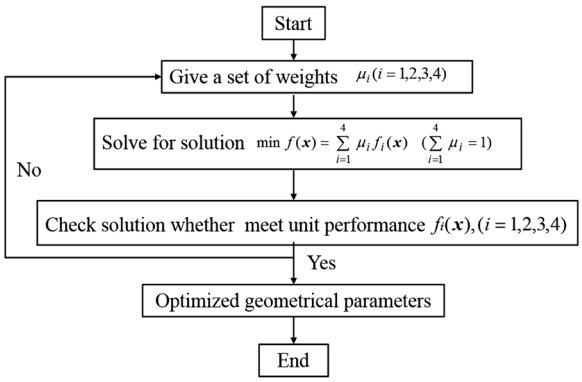


Fig. 4. Sequences of the multi-objective optimization.

One may see that $\sigma_{HM}$ can get a great value when both $\sigma_{\max}$ and $\sigma_{\min}$ get great values. $\sigma_{HM}$ can be used to evaluate the accelerating/decelerating performance of one manipulator. Moreover, this index can reflect the isotropy of dynamic performance.[28]

Considering that $\sigma_{HM}$ varies with the configuration of the manipulator, a global index similar to that proposed by Gosselin and Angeles[3] is used as one of the global performance measures to be maximized in the optimal design of the parallel manipulator. The index can be expressed as

$$\Gamma_{HM}=\frac{\int_W \sigma_{HM}dW}{\int_W dW} \tag{41}$$

The bigger the value of $\Gamma_{HM}$, the better the dynamic performance of the manipulator. In this paper, this index is used to evaluate the dynamic performance.

## 5. Optimum Design and Discussion

### *5.1. Multi-objective optimization*

A parallel manipulator with maximum possible workspace may have undesirable characteristics such as low stiffness or resonance frequencies, which means that a multi-objective optimization is needed.[29–31] In this paper, workspace, conditioning performance, accuracy and dynamic performance are considered and the multi-objective optimization problem can be expressed as

$$\min f(\boldsymbol{x})=\left[f_1(\boldsymbol{x}),f_2(\boldsymbol{x}),f_3(\boldsymbol{x}),f_4(\boldsymbol{x})\right] \tag{42a}$$

subject to

$$l_1+l+l_2\le L \tag{42b}$$

$$0<l_1<L,\ 0<l<L,\ 0<l_2<L \tag{42c}$$

where $\boldsymbol{x}$ is the vector of designed parameters $[l_1, l, l_2]$, $f_1(x)$, $f_2(x)$, $f_3(x)$ and $f_4(x)$ are the optimized objective functions of workspace, conditioning performance, accuracy and dynamic performance, respectively.

In order to solve the multi-objective optimization problem, the weighted summation method is used to translate the multi-objective optimization to single-objective optimization. Then, the solution to the comprehensive performance is determined using weighted computation. The optimization problem can be rewritten as

$$\min f(\boldsymbol{x})=\sum_{i=1}^{4}\mu_i f_i(\boldsymbol{x})\quad\left(\sum_{i=1}^{4}\mu_i=1\right) \tag{43}$$

where $\mu_i$ is the weight placed upon $f_i$. The weight not only deals with the unit objective function of the performance indexes but also indicates the priority of the performance requirements. The weight is different at different performance requirements and can be determined as shown in Fig. 4.

https://doi.org/10.1017/S0263574719001255 Published online by Cambridge University Press

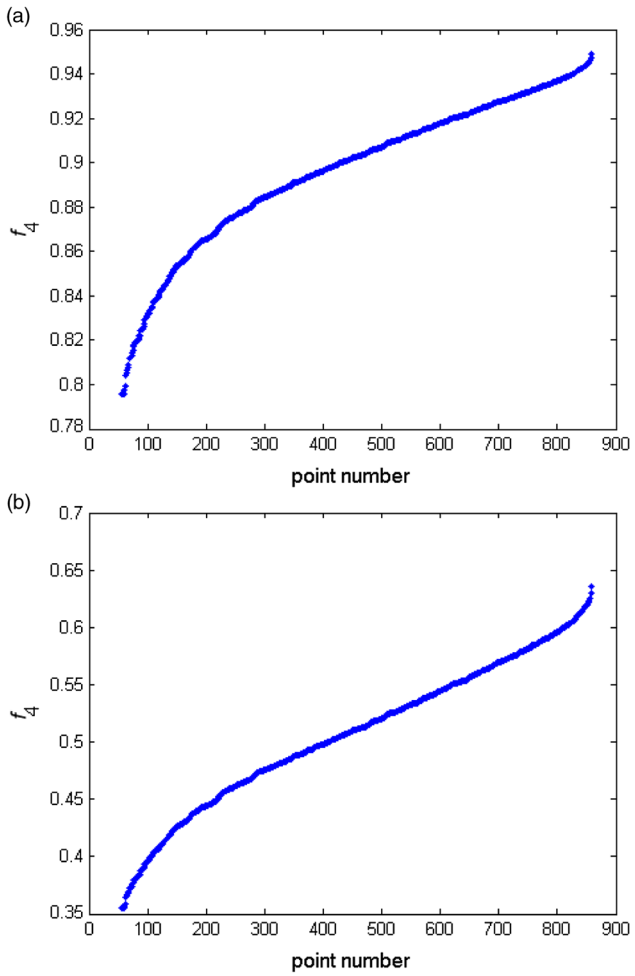


Fig. 5. Objective function of dynamic performance: (a) $f_4$ computed from Eq. (44); (b) $f_4$ computed from Eq. (45).

Since the dimensions of $f_1, f_2, f_3$ and $f_4$ are different, $f_i(x)$ should be transferred to a dimensionless function. For convenience, the objective function is redefined as

$$f_1(\boldsymbol{x}) = \frac{\Delta\bar{y}_{\max} - \Delta\bar{y}}{\Delta\bar{y}_{\max} - \Delta\bar{y}_{\min}}, f_2(\boldsymbol{x}) = \frac{\eta_{J\max} - \eta_J}{\eta_{J\max} - \eta_{J\min}}, f_3(\boldsymbol{x}) = \frac{\eta_E - \eta_{E\min}}{\eta_{E\max} - \eta_{E\min}}, f_4(\boldsymbol{x}) = \frac{\Gamma_{HM\max} - \Gamma_{HM}}{\Gamma_{HM\max} - \Gamma_{HM\min}} \tag{44}$$

where $\Delta\bar{y}_{\max}$ and $\Delta\bar{y}_{\min}$ are the maximum and minimum values of $\Delta\bar{y}$, $\eta_{J\max}$ and $\eta_{J\min}$ are the maximum and minimum values of $\eta_J$, $\eta_{E\max}$ and $\eta_{E\min}$ are the maximum and minimum values of $\eta_E$, $\Gamma_{HM\max}$ and $\Gamma_{HM\min}$ are the maximum and minimum values of $\Gamma_{HM}$, respectively. One may see that $f_1, f_2, f_3$ and $f_4$ range from 0 to 1. When $f_1, f_2, f_3$ and $f_4$ are equal to 0, the parallel manipulator has the best conditioning performance, workspace, accuracy and dynamic performance. On the contrary, the conditioning performance, workspace, accuracy and dynamic performance are the worst when $f_1, f_2$, $f_3$ and $f_4$ are equal to 1. $l_1$, $l$ and $l_2$ range from 0 to $L$ and form a design space $W_d$.

Eq. (43) shows the objective function of the optimization problem and there are many possible solutions. In this paper, the genetic algorithm is used to find the optimal solution. In genetic algorithm, the individuals are randomly selected. So the distribution of solutions which is crowding degree has a great influence on the operation of genetic algorithm. Furthermore, the objective function has an effect on the convergence speed and optimal solution. Inappropriate objective functions may lead to a local optimum solution. Therefore, the distribution of objective function $f_i(x)$ in Eq. (44) is observed. And among them, $f_4$ is pretreated by a logarithmic function.

https://doi.org/10.1017/S0263574719001255 Published online by Cambridge University Press

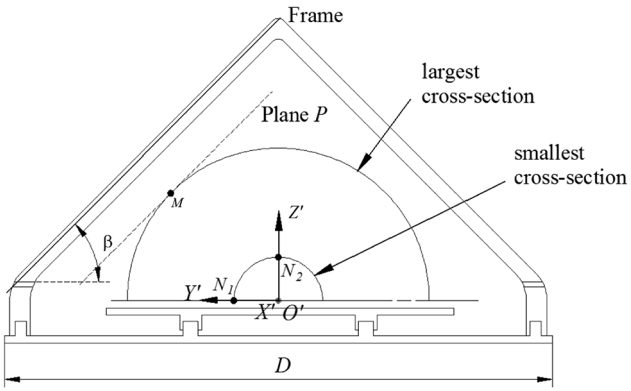


Fig. 6. Main view of the spray-painting equipment.

Here, 1000 nodes are equally meshed in $W_d$ and the dynamic index $f_4$ is evaluated at each node, as shown in Fig. 5(a). It can be seen that $f_4$ does not have a linear distribution, especially for data before point number 200, where the value is lower and means a better dynamic performance than that after point number 200. Approximately, it can be observed that $f_4$ has a logarithmic distribution. If $f_4$ is linear with respect to nodes in the design space, the optimal result using genetic algorithm is more reliable. It is reasonable to redefine $f_4$ to obtain the linear relationship between $f_4$ and nodes. Taking the logarithm of $\Gamma_{HM}$ leads to

$$f_4(\boldsymbol{x}) = \frac{\ln(\Gamma_{HM\,\max}) - \ln(\Gamma_{HM})}{\ln(\Gamma_{HM\,\max}) - \ln(\Gamma_{HM\,\min})} \tag{45}$$

Based on Eq. (45), the distribution of $f_4$ in the design space $W_d$ is shown in Fig. 5(b). A linear relationship between $f_4$ and nodes in the design space is obtained and $f_4$ given in Eq. (45) will be used as the objective function to evaluate the dynamic performance in the optimal design.

### *5.2. Design result of the frame*

Besides the geometrical parameters of the 3-DOF parallel manipulator, the geometrical parameters of the gantry frame can also impact the workspace of the spray-painting equipment. For a triangular gantry frame, there are two parameters to be optimized, namely $\beta$ and $D$, as shown in Fig. 6. From Fig. 6, one may see that $\beta$ affects the maximum spraying distance in the direction of $Y$ axis. Once $\beta$ is determined, $D$ can be determined according to geometrical relationship.

In application, the conical object can be divided into two parts to be sprayed thanks for its symmetrical architecture. Fig. 6 gives the main view of the spray-painting equipment with a large conical object to be sprayed. The diameters of the largest and smallest circular cross section of the cone are $d_1$ and $d_2$, respectively. The length of the cone is $l_b$. The coordinate $O'$-$X'Y'Z'$ is attached to the center of the largest cross section at one end of the cone object. The $X'$ axis is along the axial axis of the cone object and $Y'$ axis is horizontal. The plane $P$ is parallel to the gantry frame, which is an auxiliary plane to find $\beta$ and $D$. $M$ is the nearest spraying point in the direction of $Y$-axis, which is the tangent point of plane $P$ and the largest cross section. $N_i$ is the farthest spraying point, which is at the bottom or top of the smallest cross section. Then the coordinates of $M$ and $N_i$ can be determined and the spraying distance in the direction of $Y$-axis can be expressed as

$$\vec{N_iM} = \begin{cases} \left(-l_b,\ \frac{d_1}{2}\sin\beta - \frac{d_2}{2},\ \frac{d_1}{2}\cos\beta\right) & i = 1(0^\circ \le \beta < 45^\circ) \\ \left(-l_b,\ \frac{d_1}{2}\sin\beta,\ \frac{d_1}{2}\cos\beta - \frac{d_2}{2}\right) & i = 2(45^\circ \le \beta < 90^\circ) \end{cases} \tag{46}$$

$$\Delta y_i = \vec{N_iM}\cdot\vec{n} = \begin{cases} \left(\frac{d_1}{2}\sin\beta - \frac{d_2}{2}\right)\sin\beta + \frac{d_1}{2}\cos^2\beta & i = 1(0^\circ \le \beta < 45^\circ) \\ \frac{d_1}{2}\sin^2\beta + \left(\frac{d_1}{2}\cos\beta - \frac{d_2}{2}\right)\cos\beta & i = 2(45^\circ \le \beta < 90^\circ) \end{cases} \tag{47}$$

where $\vec{N_iM}$ is the vector from the nearest spraying point to the farthest spraying point, $\vec{n} = (0, \sin\beta, \cos\beta)$ is the unit normal vector of the plane $P$ and $\Delta y_i$ is the maximum spraying distance in the direction of $Y$-axis. The smaller the value of $\Delta y_i$, the easier it is for the equipment

https://doi.org/10.1017/S0263574719001255 Published online by Cambridge University Press

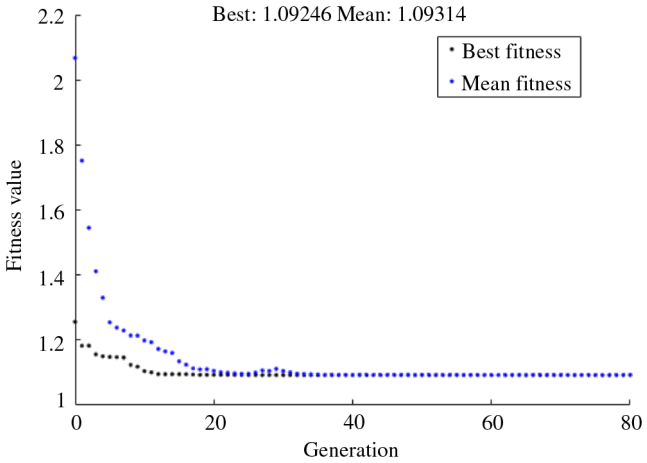


Fig. 7. Genetic algorithm adaptability changes.

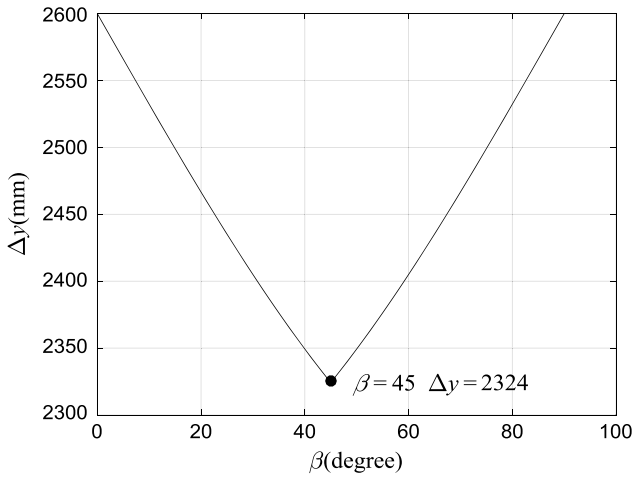


Fig. 8. The relationship between $\Delta y_i$ and $\beta$.

to finish the spray-painting work of the conical object. Thus, it is expected that $\Delta y_i$ gets a minimum value in the design. It is assumed that $d_1 = 5000$ mm, $d_2 = 729$ mm and $l_b = 6000$ mm. Based on Eqs. (46) and (47), the value of $\Delta y_i$ can be obtained, as shown in Fig. 8. When $\beta$ is smaller than 45°, $\Delta y_i$ is inversely proportional to $\beta$. When $\beta$ is greater than 45°, $\Delta y_i$ increases with the increase in $\beta$. When $\beta = 45°$, $\Delta y_i$ reaches the minimum value 2.324 m. Therefore, the optimal value for $\beta$ is 45°.

After $\beta$ is determined, $D$ can be calculated as

$$D = 2 \times \frac{\frac{d_1}{2} + \mu l_0}{\sin \beta} \tag{48}$$

where $l_0$ is the length of the spray gun, $\mu$ is the safety coefficient defined subjectively to avoid interference. If it is specified as $l_0 = 0.5$ m and $\mu = 2$, the value of $D$ is 10.18 m.

### *5.3. Design result of the 3-DOF parallel manipulator*

Besides the geometrical parameters, the inertia parameters are also used in $\Gamma_{HM}$. It is assumed that the material is evenly distributed and the mass can be computed through multiplying density by volume. If the cross section is given, only the geometrical parameters are unknown and should be determined in $\Gamma_{HM}$. The cross-section parameters of links can be optimized by stiffness analysis. In this paper, the cross section of link is a rectangle of 0.04 $m^2$ in area. The material is iron and the density is 7800 $kg/m^3$. Thus, it is reasonable to only consider the geometrical parameters in the multi-objective optimization design. The choice of $L$ is related to required range of $y$, which is determined by the size

https://doi.org/10.1017/S0263574719001255 Published online by Cambridge University Press

Table I. Geometric parameters and objective functions.

| | Geometric parameters | | | Objective functions | | | | Sum |
|---|---|---|---|---|---|---|---|---|
| **Result** | $l_1$ | $l$ | $l_2$ | $f_1(\mathbf{x})$ | $f_2(\mathbf{x})$ | $f_3(\mathbf{x})$ | $f_4(\mathbf{x})$ | $f(\mathbf{x})$ |
| 1 | 0.124 | 0.1 | 0.1 | 0.9853 | 0.1159 | 0.0570 | 0.0074 | 1.1656 |
| 2 | 3.81 | 1.076 | 3.109 | 0.2602 | 0.2064 | 0.1013 | 0.4708 | 1.0387 |

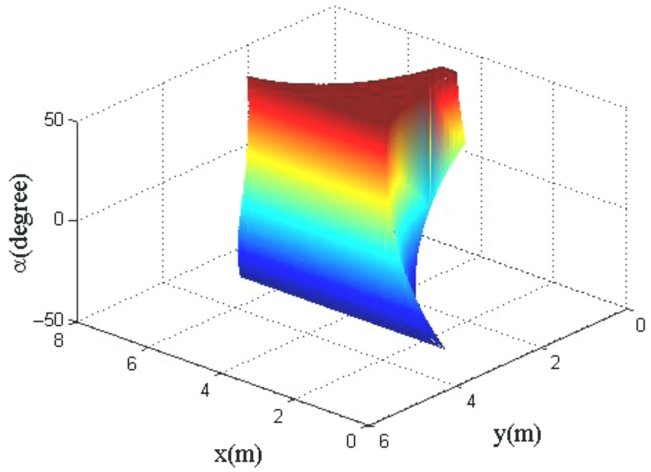


Fig. 9. 3D workspace of optimized mechanism: (a) optimized parameters and (b) randomly selected parameters.

$d_1$ and $d_2$ of the work piece to be sprayed. In combination with the workspace analysis, the length of the guide way $L$ is specified as 8 m.

Since the performance indices of workspace, conditioning, accuracy and dynamics are equally important and each objective function $f_i(x)$ has a linear distribution, it is defined that the weight $\mu_i = 0.25$ $(i = 1, 2, 3, 4)$. Based on Eq. (45), the optimal parameters can be obtained by means of Eq. (43) solved by the genetic algorithm of MATLAB optimization toolbox. Fig. 7 gives the best fitness and mean fitness values in each generation versus iteration number during the optimization process. In this paper, fitness function is constructed as Eq. (43), which is simple and efficient. The blue dots represent the mean fitness values and black dots represent the best fitness values. It can be seen that mean fitness values in each generation go down quickly and stay stable after the $40^{th}$ generation. The genetic algorithm converges quickly and optimized results are obtained with $l_1$, $l$ and $l_2$ being 3.81, 1.076 and 3.109 m, respectively. If $f_4$ without pretreatment is chosen as the objective function, the optimal parameters can be obtained by the optimization toolbox with $l_1$, $l$ and $l_2$ being 0.124, 0.1 and 0.1 m, respectively.

Table I shows the two groups of geometric parameters and the corresponding objective function values computed from Eqs. (43) and (44). It can be seen that the first group of parameters sacrifice the workspace performance to get a small $f(x)$. Compared with the second group of parameters, it converges toward a local optimum, which does not meet the workspace requirement obviously and is quite far away from the optimal design solution. The validity of the pretreatment of the objective function is verified in Table I.

Based on the second group of optimized parameters, the optimized solution is checked by the workspace, conditioning performance, accuracy and dynamic performance. The 3D workspace of the parallel manipulator is shown in Fig. 9.

In order to illustrate the effect of parameter optimization, a set of rational designed parameters ($l_1$= 3 m, $l_2 = 2$ m, $l_3 = 3$ m) are randomly chosen to analyze the workspace, conditioning performance, accuracy performance and dynamic performance and the comparison. The comparison of 2D workspace between optimized parameters and randomly selected parameters is shown in Fig. 10. The rectangular region (black line) in Fig. 10(a) is the task space to paint the surface of the conical object. In the task workspace, $y$ and $\alpha$ range from 0.4 m and 0° to 2.8 m and 30°, and it can meet the painting

https://doi.org/10.1017/S0263574719001255 Published online by Cambridge University Press

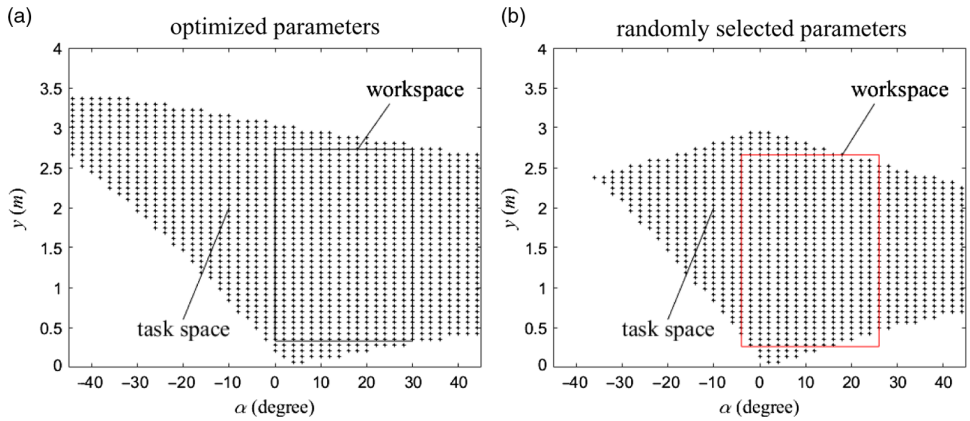


Fig. 10. 2D workspace of mechanism.

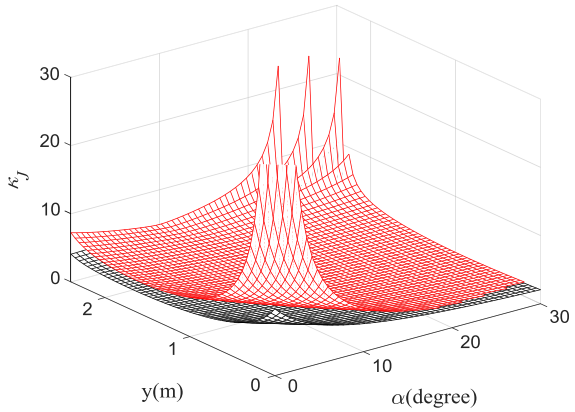


Fig. 11. Distribution comparison of conditioning performance in task space.

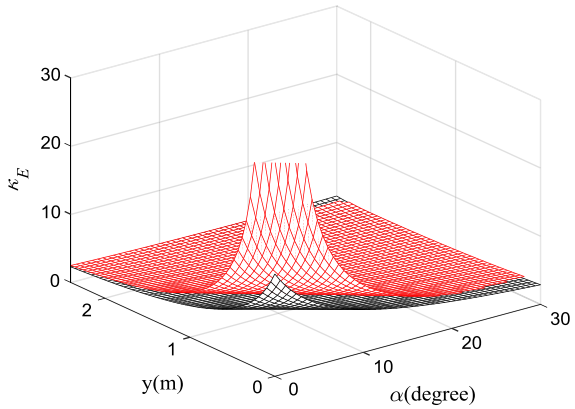


Fig. 12. Distribution comparison of accuracy performance in task space.

requirement with $\Delta y = 2.4$ m and $\Delta\alpha = 30°$. The rectangular region (red line) in Fig. 10(b) is a task space with $\Delta y = 2.4$ m and $\Delta\alpha = 30°$. In the task workspace, $y$ and $\alpha$ range from 0.33 m and $-4°$ to 2.73 m and 26°, and it can be seen that the workspace of the randomly selected parameters cannot meet the painting requirement.

The distribution comparisons of conditioning performance, accuracy and dynamic performance in task space are shown in Figs. 11–13. The black line in Figs. 11–13 represents performance contribution of optimized parameters and the red line represents performance contribution of randomly selected parameters. It can be seen from Figs. 11 and 12 that the conditioning performance and accuracy performance of optimized parameters are better than those of randomly selected parameters in

https://doi.org/10.1017/S0263574719001255 Published online by Cambridge University Press

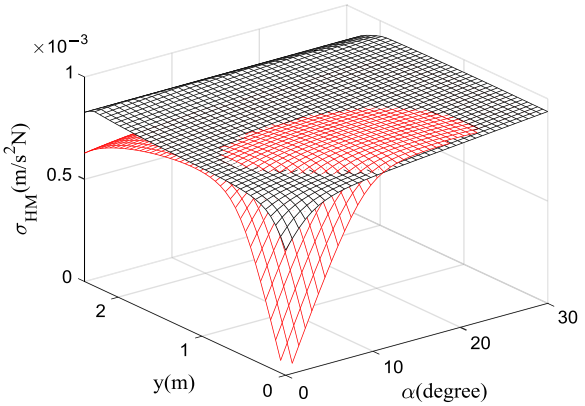


Fig. 13. Distribution comparison of dynamic performance in task space.

the whole task space, especially near the diagonal boundary region. In Fig. 13, the dynamic performance of randomly selected parameters is worse in more than half of the task space and deteriorates sharply in the boundary in task space.

For the surface painting of the conical object, the bus of cone can be approximated as a parabolic. This requires that the spray-painting mechanism has a good performance in a diagonal region in $y$-$\alpha$ workspace. From Figs. 11–13, one may see that there is a diagonal region from diagonal points $\alpha = 0°$, $y = 2.8$ m to $\alpha = 30°$, $y = 0.4$ m that the conditioning performance, accuracy and dynamic performance have no obvious change. Therefore, the manipulator has a uniform conditioning performance, accuracy and dynamic performance in the spray-painting of the conical object and a high-quality spray-painting can be expected. Hence, the optimized solution obtained using the genetic algorithm has improved the overall performance. Genetic algorithm method in this paper demonstrates the obvious advantages in simplicity and efficiency.

## 6. Conclusions

In this paper, a spray-painting equipment that consists of a feed worktable, a gantry frame and two serial–parallel manipulators is presented and the optimal design of the 3-DOF parallel manipulator in the spray-painting equipment is investigated. The conditioning performance, workspace, accuracy performance and dynamic performance indices are considered in the optimal design using weighted sum method with genetic algorithm toolbox. Furthermore, the geometrical parameters of the gantry frame are also optimized. Taking the conical object with the length being 6 m as painted object, the geometrical parameters of the parallel manipulator and the gantry frame are determined. After optimization, the parallel manipulator has a good workspace, conditioning, accuracy and dynamic performance and a high-quality spray-painting can be expected. This work is of great significance for the actual manufacture of the spray-painting equipment for painting a long object with conical surface.

## Acknowledgment

This work is supported by Beijing Natural Science Foundation (Grant No. 3194050), the China Postdoctoral Science Foundation (Grant No. 2018M631455), the National Natural Science Foundation of China (Grant No. 51622505 and 51575307), Top-Notch Young Talents Program of China and Tianjin Key Laboratory of High Speed Cutting & Precision Machining.

## References

1. Y. Q. Yu, Z. C. Du, J. X. Yang and Y. Li, "An experimental study on the dynamics of a 3-RRR flexible parallel robot," *IEEE Trans. Rob.* **27**(5), 992–997 (2011).
2. J. Wu, X. L. Chen and L. P. Wang, "Design and dynamics of a novel solar tracker with parallel mechanism," *IEEE-ASME Trans. Mechatr.* **21**(1), 88–97 (2016).
3. C. Gosselin and J. Angeles, "The optimal kinematic design of a planar three-degree-of-freedom parallel manipulator," *J. Mech. Transm. Autom. Des.* **110**(1), 35–41 (1988).
4. G. Yu, J. Wu and L. Wang, "Stiffness model of a 3-DOF parallel manipulator with two additional legs," *Int. J. Adv. Rob. Syst.* **11**(10), 173 (2014).

https://doi.org/10.1017/S0263574719001255 Published online by Cambridge University Press

5. G. Yu, L. Wang, J. Wu, D. Wang and C. Hu, "Stiffness modeling approach for a 3-DOF parallel manipulator with consideration of nonlinear joint stiffness," *Mech. Mach. Theory* **123**, 137–152 (2018).
6. L. Wang, G. Yu and J. Wu, "A comparison study on the stiffness and natural frequency of a redundant parallel conveyor and its nonredundant counterpart," *Adv. Mech. Eng.* **9**(11), 1687814017733690 (2017).
7. J. Wu, J. Wang, L. Wang and T. Li, "Dynamics and control of a planar 3-DOF parallel manipulator with actuation redundancy," *Mech. Mach. Theory* **44**(4), 835–849 (2009).
8. H. R. M. Daniali, P. J. Zsombormurray and J. Angeles, "Singularity analysis of planar parallel manipulators," *Mech. Mach. Theory* **30**(5), 665–678 (1995).
9. I. A. Bonev, D. Zlatanov and C. M. Gosselin, "Singularity analysis of 3-DOF planar parallel mechanisms via screw theory," *Trans. ASME J. Mech. Des.* **125**(3), 573–581 (2003).
10. Z. M. Ji, "Study of planar three-degree-of-freedom 2-RRR parallel manipulators," *Mech. Mach. Theory* **38**(5), 409–416 (2003).
11. S. K. Ider, "Singularity robust inverse dynamics of planar 2-RPR parallel manipulators," *Proc. Inst. Mech. Eng. C J. Mech. Eng. Sci.* **218**(7), 721–730 (2004).
12. T. Huang, M. Li, Z. Li, D. G. Chetwynd and D. J. Whitehouse, "Optimal kinematic design of 2-DOF parallel manipulators with well-shaped workspace bounded by a specified conditioning index," *IEEE Trans. Rob. Autom.* **20**(3), 538–543 (2004).
13. Z. F. Shao, X. Q. Tang, L. P. Wang and D. F. Sun, "Atlas based kinematic optimum design of the Stewart parallel manipulator," *Chin. J. Mech. Eng.* **28**(1), 20–28 (2015).
14. R. Kelaiaia, A. Zaatri and O. Company, "Multiobjective optimization of 6-dof UPS parallel manipulators," *Adv. Rob.* **26**(16), 1885–1913 (2012).
15. T. Huang, Z. X. Li, M. Li, D. G. Chetwynd and C. M. Gosselin, "Conceptual design and dimensional synthesis of a novel 2-DOF translational parallel robot for pick-and-place operations," *J. Mech. Des.* **126**(3), 449–455 (2004).
16. Q. Xu and Y. Li, "Design and analysis of a new singularity-free three-prismatic-revolute-cylindrical translational parallel manipulator," *Proc. Inst. Mech. Eng. C J. Mech. Eng. Sci.* **221**(5), 565–577 (2007).
17. F. Hao and J. P. Merlet, "Multi-criteria optimal design of parallel manipulators based on interval analysis," *Mech. Mach. Theory* **40**(2), 157–171 (2005).
18. X. J. Liu, J. Li and Y. H. Zhou, "Kinematic optimal design of a 2-degree-of-freedom 3-parallelogram planar parallel manipulator," *Mech. Mach. Theory* **87**, 1–17 (2015).
19. R. Kelaiaia, O. Company and A. Zaatri, "Multiobjective optimization of a linear delta parallel robot," *Mech. Mach. Theory* **50**, 159–178 (2012).
20. J. Wu, X. L. Chen, L. P. Wang and X. J. Liu, "Dynamic load-carrying capacity of a novel redundantly actuated parallel conveyor," *Nonlinear Dynam.* **78**(1), 241–250 (2014).
21. J. S. Zhao, F. L. Chu and Z. J. Feng, "Singularities within the workspace of spatial parallel mechanisms with symmetric structure," *Proc. Inst. Mech. Eng. C J. Mech. Eng. Sci.* **224**(2), 459–472 (2010).
22. J. P. Merlet, "Jacobian, manipulability, condition number, and accuracy of parallel robots," *Trans. ASME J. Mech. Des.* **128**(1), 199–206 (2006).
23. C. Wu, X. J. Liu, L. Wang and J. Wang, "Optimal design of spherical 5R parallel manipulators considering the motion/force transmissibility," *J. Mech. Des.* **132**(3), 31002–31010 (2010).
24. X. J. Liu, J. Wang and G. Pritschow, "On the optimal kinematic design of the PRRRP 2-DoF parallel mechanism," *Mech. Mach. Theory* **41**(9), 1111–1130 (2006).
25. O. Ma and J. Angeles, "Optimum Architecture Design of Plat-Form Manipulators," *Fifth International Conference on IEEE Robots in Unstructured Environments*, ICAR, Pisa (1991) pp. 1130–1135.
26. Q. Xu and Y. Li, "Error analysis and optimal design of a class of translational parallel kinematic machine using particle swarm optimization," *Robotica* **27**(1), 67–78 (2009).
27. S. K. Ider, "Singularity robust inverse dynamics of planar 2-RPR parallel manipulators," *Proc. Inst. Mech. Eng. C J. Mech. Eng. Sci.* **218**(7), 721–730 (2004).
28. J. Wu, Y. Gao, B. Zhang and L. Wang, "Workspace and dynamic performance evaluation of the parallel manipulators in a spray-painting equipment," *Rob. Comput. Integr. Manuf.* **44**, 199–207 (2017).
29. I. Tyapin and G. Hovland, "Kinematic and elastostatic design optimisation of the 3-DOF Gantry-Tau parallel kinematic manipulator," *Model. Identif. Control* **30**(2), 39–56 (2009).
30. R. E. Stamper, L. W. Tsai and G. C. Walsh, "Optimization of a Three DOF Translational Platform for Well-Conditioned Workspace," *Proceedings of International Conference Robotics and Automation* New Mexico, vol. 4 (1997) pp. 3250–3255
31. J. S. Zhao, X. Liu, Z. J. Feng and J. S. Dai, "Design of an Ackermann type steering mechanism," *Proc. Inst. Mech. Eng. C J. Mech. Eng. Sci.* **227**(11), 2549–2562 (2013).